17th World Conference on Earthquake Engineering, 17WCEE
Sendai, Japan - September 13th to 18th 2020

Experimental Study of Sliding Friction Damper for High-Performance Steel Structures

M. Paronesso[1], D.G. Lignos[2]

[1] *Doctoral assistant, École polytechnique fédérale de Lausanne, EPFL, Resilient Steel Structures Laboratory, EPFL-ENAC-IIC-RESSLab, Station 18, CH-1015 Lausanne, Switzerland, martina.paronesso@epfl.ch*
[2] *Associate professor, École polytechnique fédérale de Lausanne, EPFL, Resilient Steel Structures Laboratory, EPFL-ENAC-IIC-RESSLab, Station 18, CH-1015 Lausanne, Switzerland, dimitrios.lignos@epfl.ch*

Abstract

Passive energy dissipation devices are widely utilized in buildings to minimize structural and non-structural damage under seismic loading. Commonly used devices include, among others, yield, viscous and friction dampers. While the use of yield dampers, such as buckling-restrained braces (BRBs), has been fairly well established in the earthquake engineering practice, arguably, uncertainties regarding the amount of cyclic hardening of the BRB yield core necessitate the BRB qualification testing for the design of the BRB's non-dissipative elements. An additional concern may be the residual deformations along the building height in the aftermath of earthquakes. Similarly, viscous dampers may exert forces that are influenced by the dynamic load imposed on a building due to their sensitivity to temperature and imposed velocity. Maintenance of viscous dampers due to potential leakage may be another complexity.

While friction dampers do not generally experience the aforementioned issues, their use in seismic applications is still evolving. One reason could be that their performance is strongly dependent on the selected friction pad material type. Ideally, friction pads should have a static friction coefficient between 0.3 and 0.4 under high-pressure (between 10 and 20 MPa). They should also exhibit stable force-displacement hysteretic response under cyclic loading. All-in-all, the selection of a suitable friction pad material for structural applications is non-trivial.

In this regard, friction pads commonly used in braking applications of the automobile industry may be effective to address long-term effects associated with corrosion and delamination of friction pads. In order to investigate their applicability in the context of seismic engineering, a sliding friction damper prototype is developed and tested under various loading histories at the EPFL Structures Laboratory. The damper is designed for a maximum axial force of 450 kN and can accommodate a maximum axial displacement of ± 80 mm.

The force-displacement response of the friction damper is investigated by testing two friction pad types under two different pressure levels at the sliding interface. Cyclic tests with constant and increasing amplitudes are conducted at different rates to depict their influence on the force-displacement response of the friction damper. Furthermore, a pulse-like loading protocol is carried out in order to test the friction damper under conditions similar to those of an actual seismic event. The evolution of the static and dynamic friction coefficients is examined by monitoring both the sliding force and bolt preload.

The experimental results suggest that under sliding motion, the examined friction pads provide a fairly constant sliding force, thereby exhibiting similar static and dynamic friction coefficients. Furthermore, the force-displacement hysteretic response of the friction damper is fairly stable and repeatable. Finally, similar static friction coefficients are obtained for different slip loads and sliding velocities, suggesting that the behavior of the tested friction pads is nearly pressure- and velocity-independent.

Keywords: friction damper, friction coefficient, high-performance steel structures, passive control

1. Introduction

In the context of earthquake engineering, friction dampers are utilized to provide supplemental energy dissipation to structures aiming to control structural and non-structural damage in the aftermath of earthquakes. The performance of friction dampers strongly depends on the friction properties of the respective materials utilized at the damper's sliding interfaces. In the past forty years, numerous experimental investigations have been conducted on different types of friction pads. In [1], among others, a summary of available friction damper options for the seismic protection of steel buildings can be found. Tirca [2] provides a comprehensive experimental study in which the effectiveness of various solutions in mitigating the seismic demands in structures is carefully examined.

Several studies have focused on mild-steel friction pads [3]-[8]. The experimental findings have demonstrated that the latter may exhibit an unstable force-displacement hysteretic response. Moreover, the friction pads exhibit severe surface damage due to wear. Other researchers have investigated the use of brass [4], [5], [7], [8]. Although their hysteretic response is found to be stable compared to mild-steel pads, their use in contact with steel plates could potentially be problematic due to galvanic corrosion. Further investigations have been conducted on steel plates coated with sprayed aluminum [7], [9], [10]. This solution provides a fairly stable force-displacement hysteretic response of the friction device. However, the obtained friction coefficients turn out to be somewhat pressure dependent. Furthermore, the application process of the coating is non-trivial. It usually requires specialized equipment to ensure a high-quality control and performance of the coated steel plates and associated sliding interfaces.

In recent work, Bissaloy steel pads [5], [6], [11] have been explored as potential friction pad materials in seismic applications. Their hysteretic response is quite stable, exhibiting only minor surface degradation due to wear. Nevertheless, friction coefficients lower than 0.2 are obtained. In more recent studies [7], [12], several composite non-metallic materials have been investigated in potential friction damper applications. The acquired experimental results suggest that a few of these materials can provide considerable energy dissipation under cyclic loading. Their friction coefficient is pressure- and velocity-independent and it is typically lower than 0.2 [7].

In light of these findings, the authors focus their research on non-metallic friction pads utilized in braking applications of the automobile industry. Emphasis is placed on materials that are characterized by friction coefficients higher than 0.2. The selected materials are cost-effective and readily available on the market. In order to investigate their performance under cyclic loading, a sliding friction damper prototype is designed, fabricated and physically tested within EPFL's Structures Laboratory. The experimental campaign is conducted under two pressure levels and three cyclic loading protocols in order to infer the properties of the friction pads with regard to pressure- and velocity-dependency. In the context of this conference paper, the main outcomes obtained for two of the examined materials are discussed.

2. Text matrix

2.1 Description of the sliding friction damper

The sliding friction damper is illustrated in Fig. 1. It consists of four steel plate types made of standard manufacturing tolerances. These include, (i) end steel plates, which are positioned at the damper ends and are equipped with ball joints; (ii) an inner slotted plate, which is pierced by three 330mm long slotted holes; (iii) fixed outer steel plates that connect one of the end plates to the inner slotted plate; and (iv) sliding outer steel plates, which connect one of the end plates to the slotted holes of the inner plate. High-strength steel pins (ETG 100, $f_y \geq 865$ MPa) are utilized to connect the end plates to the outer plates, whereas 2 x 6 preloaded high-strength M24 bolts 10.9 class ($f_{ub} = 1000$ MPa) are used to join the respective components as shown in Fig. 1. Sliding motion occurs between two friction pads and the inner slotted plate.

The damper is designed according to [13] for a maximum axial force of 450 kN and a maximum axial displacement of ± 100 mm. Its expected slip load is estimated by using Coulomb's law of friction [14]:

$$F_s = n_s \cdot \mu_s \cdot N_{tot} \quad (1)$$

In which, F_s is the slip load (i.e. static friction force); n_s is the number of slip interfaces; μ_s is the static friction coefficient characterizing the friction pad; and N_{tot} is the total normal force applied by the preloaded bolts (i.e. $N_{tot} = 6 \cdot N_{bolt}$).

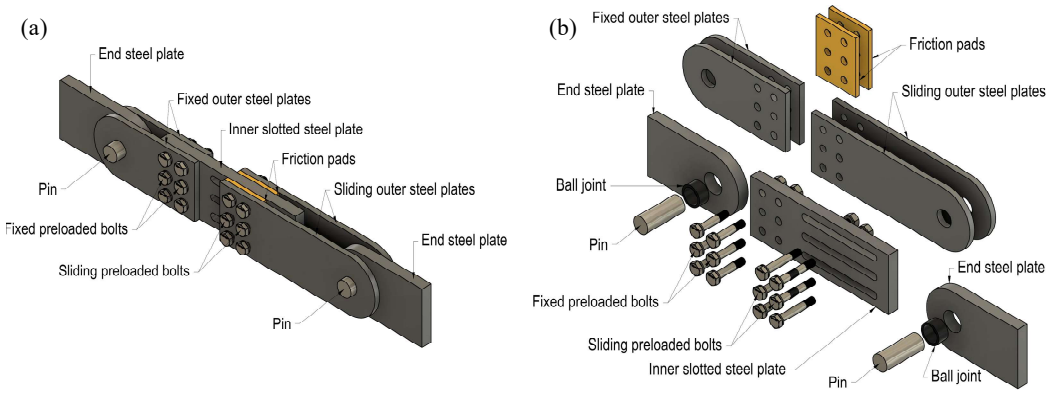

Fig. 1 – Idealized sliding friction damper: (a) 3D view of the damper assembly, (b) extruded 3D view

2.1.1 Steel components

The metal plates shown in Fig. 2a are made of S355 J2 structural steel (f_y = 355 MPa). They have a width of 220 mm and they are either 20 mm or 40 mm thick. Their geometry is shown in Fig. 2b. Each plate has standard 24 mm diameter holes with a 2 mm tolerance. The sliding motion is allowed through three 330mm long slotted holes realized in the inner plate. Six preloaded M24 structural bolts 10.9 class are utilized to apply the clamping force. Disc spring washers (SCHNORR, Φ_i = 25 mm, Φ_e = 56 mm, h = 7.75 mm, t = 6 mm) are used to maintain the bolt pretension constant during the sliding motion, thereby minimizing pretension variations due to wear (see Fig. 2c). Two high-strength steel pins (ETG 100, $f_y \geq$ 865 MPa) are utilized to realize a pinned connection at the friction damper's ends. Their main dimensions are illustrated in Fig. 2c. Ball joints (SKF GE 50 ESX-2LS, Φ_i = 50 mm, Φ_e = 75 mm) are inserted in the 75 mm diameter hole of the end plates in order to accommodate potential relative movements between the latter and the pins.

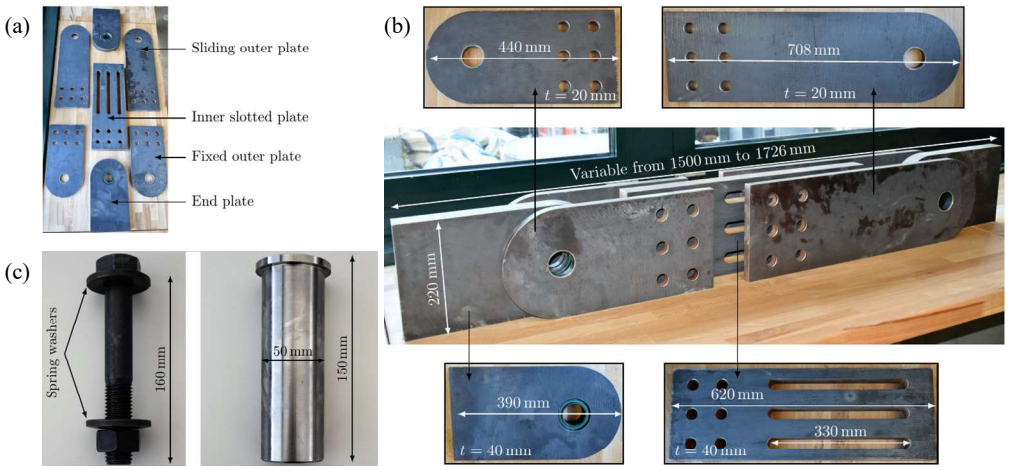

Fig. 2 – Sliding friction damper: (a) steel plates, (b) dimensions of the steel plates, (c) bolt and pin used to assemble the sliding friction damper

2.1.2 Friction pads

Friction pads, which are utilized in braking applications of the automobile industry are investigated herein. The following pre-established criteria are established prior to physical testing:

- While not a necessity, the static friction coefficient μ_s of the pads should ideally at least 0.30, in order to minimize the number of preloaded bolts to achieve the required slip load F_s (see Eq. (1)). This, in turn, affects the dimensions of the sliding friction damper.
- Under cyclic loading, the sliding friction damper should develop a stable and repeatable hysteretic response. For this purpose, the static and dynamic friction coefficients μ_s and μ_d of the friction pads should be ideally the same [15]. Furthermore, in order to limit surface wear, the hardness of the friction pads should be lower (or higher) compared to that of the steel plates [15].
- Galvanic corrosion at the slip interfaces shall be avoided, hence non-metallic composite friction pads are preferable.
- During sliding, the steel plates, which are in contact with the friction pads, should experience minimal damage. For this purpose, the hardness of the friction pads shall be lower than the one of the steel plates [15]. This criterion aims at concentrating the damage in the components that can be more easily replaced in the aftermath of earthquakes, i.e. the friction pads.
- The selected friction pads should be readily available on the market at a fairly low cost.

Within such a context, five non-metallic composite materials are selected. In this paper, the experimental results obtained for two of them are discussed. These materials are noted as M1 and M2 hereinafter. The dimensions of the respective friction pads are illustrated in Fig. 3. According to the manufacturer specifications, the static friction coefficient of M1 is nearly equal to 0.59 under a maximum operating pressure of 1.72 MPa (μ_d is not provided). Conversely, M2 is characterized by a μ_s value of approximately 0.36 under a reference pressure of 1 MPa. In this case, the dynamic friction coefficient was provided *a priori*. It is relatively similar to the static one (i.e. μ_d = 0.32 under a pressure of 1 MPa).

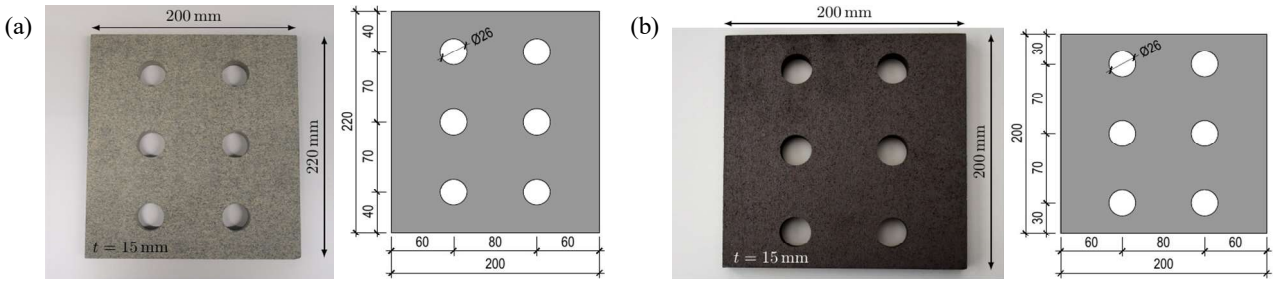

Fig. 3 – Friction pads: (a) M1, (b) M2

2.2 Test apparatus

The full-scale experiments of the sliding friction damper are carried out under displacement control by means of a universal 1 MN servo hydraulic Schenck machine. Its maximum stroke is equal to 250 mm. Referring to Fig. 4, the friction damper is clamped at both extremities with a maximum pressure of 490 bars (i.e. 49 MPa). The installation process was well thought up front in such a way to ensure verticality of the device at the rest position.

The controlled displacement, δ_m, is applied by the hydraulic piston, which is positioned at the top of the damper. The axial stiffness of the Schenck machine is significantly larger than that of the friction damper prototype. As such, the test can be controlled directly from the Schenck machine's piston. However, supplemental instrumentation is installed on the friction damper to monitor a number of aspects of interest to the authors for the proper characterization of the sliding damper device. The instrumentation program is discussed in the subsequent section.

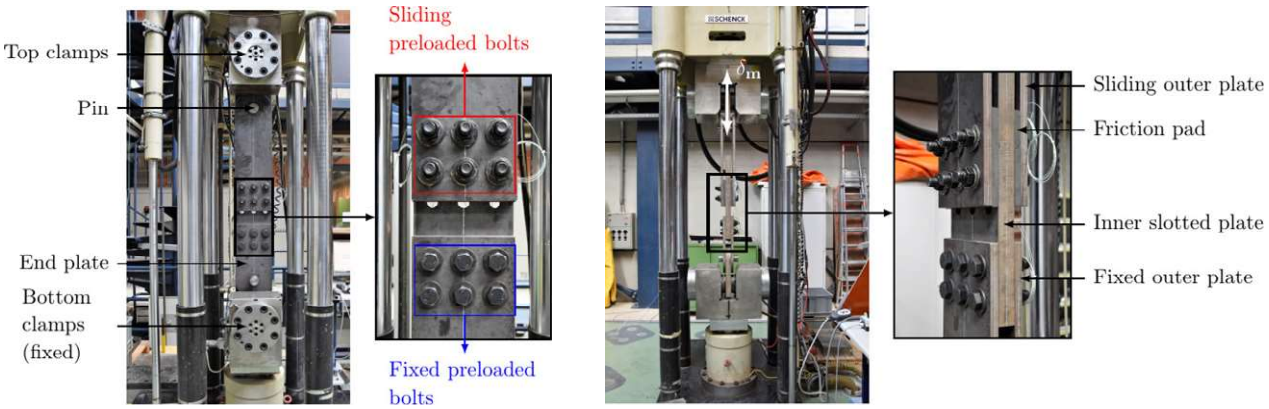

Fig. 4 – Sliding friction damper installed in the Schenck machine

2.3 Instrumentation

Figure 5 shows the instrumentation of the sliding friction damper. In total, 15 sensors are utilized, including linear variable differential transformers (LVDTs), inclinometers (INCs), thermocouples (THs) and a washer load cell (WLC). The axial force experienced by the friction damper is measured by means of a load cell positioned in the Schenck machine, whereas the axial displacement is measured with two LVDTs located on the fixed and sliding outer plates (LVDTv-W and LVDTv-E). Three additional LVDTs are used to monitor the in-plane and out-of-plane damper movements (LVDTh-WE, LVDTh-W-NS, LVDTh-E-NS). Two inclinometers are utilized to measure the damper's in-plane and out-of-plane rotations (INC-WE, INC-NS). Thermocouples are used to track the temperature variations at the surface of the inner slotted plate (THout) and close to the sliding interfaces (THbolt). A washer load cell is used to verify if pretension variations occur during the sliding motion and to get a sense of the applied bolt preload prior to testing.

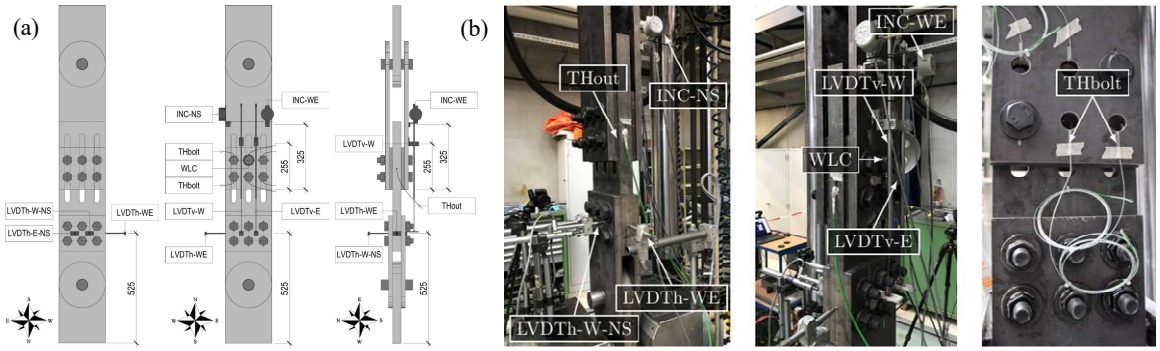

Fig. 5 – Instrumentation of the sliding friction damper: (a) drawing representation and sensor positions, (b) photos after the instrumentation installation on one of the test specimens

2.4 Loading protocols

The friction pads M1 and M2 are tested under eight different loading protocols. Herein, the experimental results obtained under three of these protocols are presented due to brevity. Notably, cyclic tests with constant and increasing amplitudes are conducted at different rates (i.e. 0.025 Hz and 0.15 Hz) in order to investigate its effect on the force-displacement response of the friction damper (see Fig. 6a and 6b). Furthermore, a pulse-like loading protocol is carried out in order to test the specimen under conditions similar to those occurring during a seismic event (see Fig. 6c). For this test, the maximum sliding velocity (i.e. $v_{s,max}$ = 27 mm/s) and the excursion associated to it (i.e. 50 mm) are constrained by the maximum capacity of the Schenck machine along with the associated oil flow of the available hydraulic pump. The loading protocol with constant amplitude (0.025 Hz) is run for an expected slip load of 150 kN and 300 kN

in order to verify if the static and dynamic friction coefficients of the pads M1 and M2 are pressure dependent. The rest of the tests are performed for F_s = 300 kN. The target F_s values are achieved by calibrating the bolt preload through a torque wrench. Details of this calibration are not shown due to brevity.

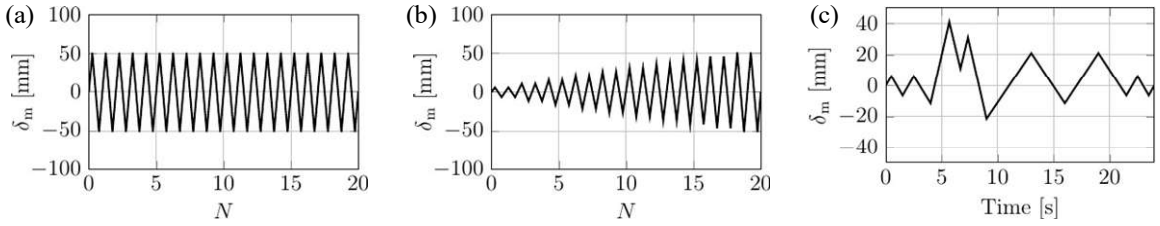

Fig. 6 – Loading protocols (a) constant amplitude (0.025 Hz), (b) increasing amplitude (i.e. 0.15 Hz), (c) pulse-like

3. Experimental results

In this section, we provide a synthesis of the experimental results. The data obtained for the expected slip loads of 150 kN and 300 kN are compared. The performance of the friction damper is evaluated in terms of axial force-axial displacement ($F - \delta$), whereas the static and dynamic friction coefficients (μ_s and μ_d) of the pads are reported as a function of the cumulative dissipated energy (ΣE_i) at each instant i. The bolt preload measurements depict any potential pretension variations during the sliding motion for each loading protocol. The effect of temperature on the friction coefficient of the pads is not discussed herein due to brevity.

3.1 Cyclic loading protocol with constant amplitude

Figure 7 shows the results obtained under the cyclic loading protocol with constant amplitude. The test conducted on M1 is interrupted during the 9th and 5th loading cycle for a F_s = 150 kN and 300kN, respectively, due to the net-section fracture of one friction pad perpendicular to the loading direction (see Figs. 7a and 7b). Interestingly, the fractured friction pad continued to dissipate energy by sliding in two/three separate parts for few additional loading cycles. While the test conducted on M2 for F_s = 150 kN does not experience friction pad fracture (see Fig. 7f), the one for F_s = 300 kN is interrupted during the 11th loading cycle due to fracture of one of the friction pads, as shown in Fig. 7g.

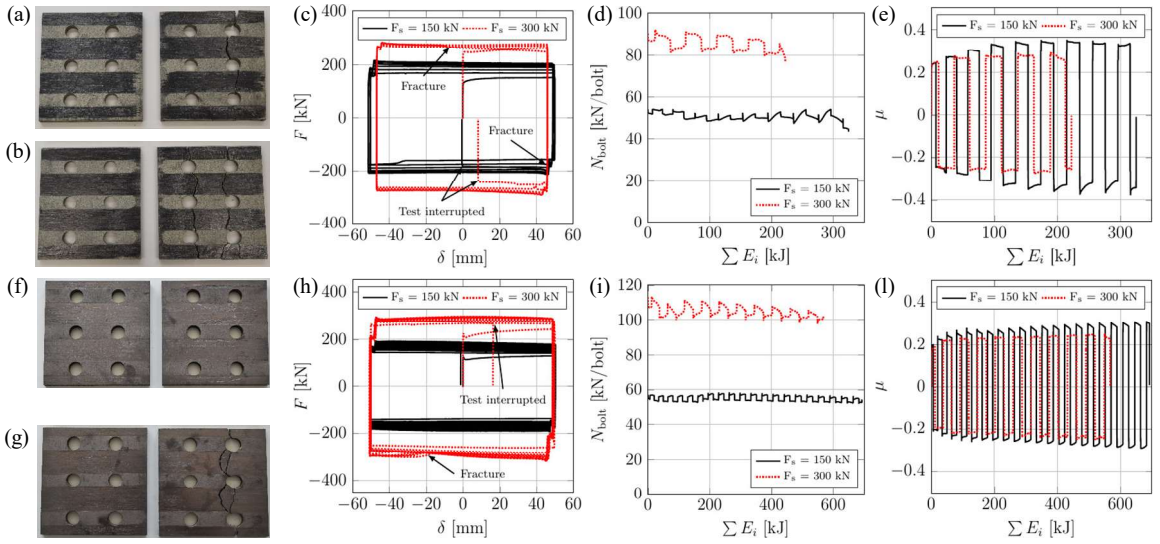

Fig. 7 – Results obtained for M1 (first row) and M2 (second row) under the cyclic loading protocol with constant amplitude (f = 0.025 Hz)

The measured response of M1 and M2 is fairly similar. Notably, Figs. 7c and 7h suggest that once the slip load is exceeded, the friction damper slides under a fairly constant axial force. This implies that μ_s and μ_d of both M1 and M2 are relatively similar. Furthermore, F slightly increases with the number of loading cycles. This phenomenon is particularly pronounced for F_s = 150 kN. A possible explanation for this behavior is illustrated in Figs. 7e and 7l. For F_s = 150 kN, the friction coefficient of M1 and M2 progressively increases with respect to ΣE_i, whereas it remains fairly stable for F_s = 300 kN. During the sliding motion, the surface of the friction pads wears and becomes rougher. Therefore, the force required to slide one surface over the other is larger than the preceding loading cycles [7]. For F_s = 150 kN, the wearing process is more evident because during the sliding motion the friction damper experiences an in-plane rotation, which is shown in Fig. 8 for one of the tests. By applying a larger clamping force, such rotation is partially restrained, thus the friction pad surface is less grooved and μ increases more gradually. However, additional factors can potentially contribute to this phenomenon and further investigations are currently under way by the authors.

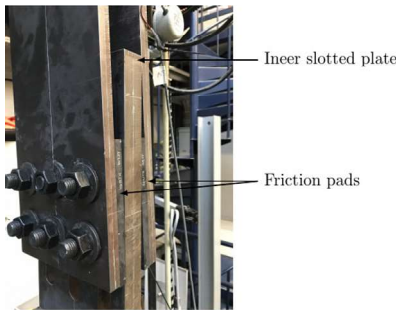

Fig. 8 – Typical in-plane rotation experienced by the sliding friction damper

The friction coefficients provided by M1 and M2 differ according to the expected slip load considered (see Figs. 7e and 7l). This suggests that the latter are somewhat pressure dependent. The effect of the clamping force on μ is further discussed in Section 4.1.

With regard to the bolt preload, N_{bolt}, Figs. 7d and 7i suggest that it remains relatively constant during the tests conducted with a slip load F_s of 150 kN. Conversely, a progressive loss of pretension load up to a maximum of about 10% is observed for F_s = 300 kN for both M1 and M2. Notwithstanding this loss, F remains fairly stable throughout the experiment due to the increase of μ. Furthermore, preload variations within ± 5% are observed for both expected slip loads. Notably, a minor increase of N_{bolt} occurs, when the applied force is reversed from tension to compression. Under compression the sliding outer plates slightly move out-of-plane, thereby increasing the normal stress in the bolts relative to that under tension.

3.2 Cyclic loading protocol with increasing amplitude

The results obtained for F_s = 300 kN under the cyclic loading protocol with increasing amplitude are illustrated in Fig. 9. The test conducted on M1 is interrupted during the 10th loading cycle because one of the friction pads fractured in its net section as shown in Fig. 9a. Conversely, the test conducted on M2 is completed without experiencing any fracture.

The force-displacement response obtained for M1 is characterized by an initial hardening phase and a subsequent stable stage, i.e. F assumes similar values under consecutive loading cycles (see Fig. 9b). Similar results are obtained for M2. However, in such a case, cyclic hardening is less pronounced. Instead, a progressive decrease of F is observed after the 35 mm loading cycle. A possible explanation for the above-mentioned behaviors is illustrated in Figs. 9d and 9h. Notably, the friction coefficient of both M1 and M2 rapidly increases during the initial loading cycles. As discussed in Section 3.1, this increase is related to a wearing process acting at the sliding interface. However, by comparing Figs. 7e and 9d (i.e. μ values obtained for M1 and F_s = 300 kN), cyclic hardening is more pronounced when increasing sliding velocities

are applied. This suggests that M1 is subjected to a visco-plastic effect, i.e. μ assumes larger values at higher loading rates [16]. Conversely, the friction coefficient of M2 exhibits minor variations under constant and increasing sliding velocities. This indicates that the latter attains a minor velocity dependence, i.e. the increase of μ observed in Fig. 9h is mainly related to a wearing process. The effect of the loading rate on μ is further investigated in Section 4.2. Following the minor hardening phase, the friction coefficients of both M1 and M2 stabilize. For M1, this stabilization is maintained up to fracture of one of the pads. In M2, a softening response is observed from the 35 mm loading cycle. This suggests that both materials can provide more-or-less constant μ values when they operate at sliding velocities that exceed 10 mm/s. This implies that in such a case, the visco-plastic effect becomes negligible for M1 (see Section 4.2). On the other hand, the surface of the pads becomes smooth under continuous sliding motion. Part of the debris falls out from the sliding interface. Consequently, the wearing process becomes less severe and μ decreases. The preload variations shown in Figs. 9c and 9g are consistent with those observed in Section 3.1. Regarding M1, the bolt preload remains stable up to the fracture of one of the friction pads. Similar results hold true for M2.

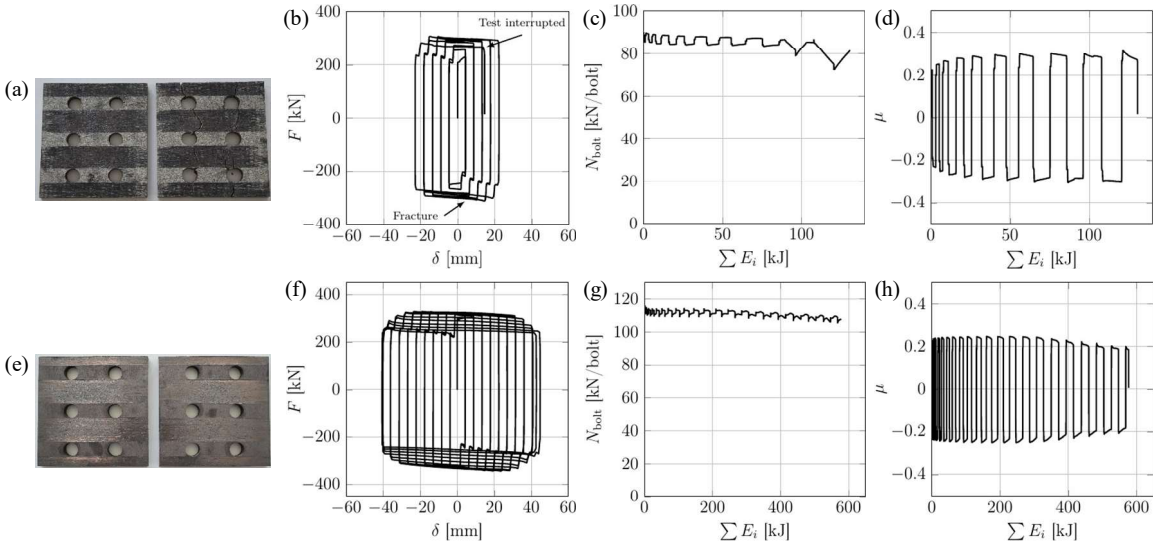

Fig. 9 – Results obtained for M1 (first row) and M2 (second row) under the cyclic loading protocol with increasing amplitude (f = 0.15 Hz) and F_s = 300 kN

3.3 Pulse-like loading protocol

The results obtained under the pulse-like loading protocol are illustrated in Fig. 10 for a targeted slip load of F_s = 300N. The test is completed for both materials without experiencing any fractures. The condition of the pads after the completion of the tests is shown in Figs. 10a and 10e for M1 and M2, respectively. The damage patterns on their surface are consistent with the previous tests described in Sections 3.1 and 3.2.

Referring to Figs. 10c and 10g, the bolt preload experiences minor variations during the test. Conversely, the friction coefficient of M1 and M2 progressively increases during the first two loading cycles. Subsequently, it achieves a constant value of 0.28 and 0.22 for M1 and M2, respectively. This value is maintained throughout the test, as shown in Figs. 10d and 10h. This corroborates the above-mentioned hypothesis that, at high sliding velocities (i.e. 27 mm/s), the visco-plastic effect is negligible for M1 and μ turns out to be stable. Consequently, the force-displacement response illustrated in Figs. 10b and 10f shows minor cyclic hardening during the first two loading cycles. However, F exhibits a fairly stable hysteretic behavior under consecutive loading cycles. Furthermore, since $\mu_s \approx \mu_d$ for both M1 and M2, F remains constant during the sliding motion. The above observations suggest that under conditions potentially similar to those occurring during a seismic event, the examined friction pads can provide a fairly stable and repeatable axial force-displacement response.

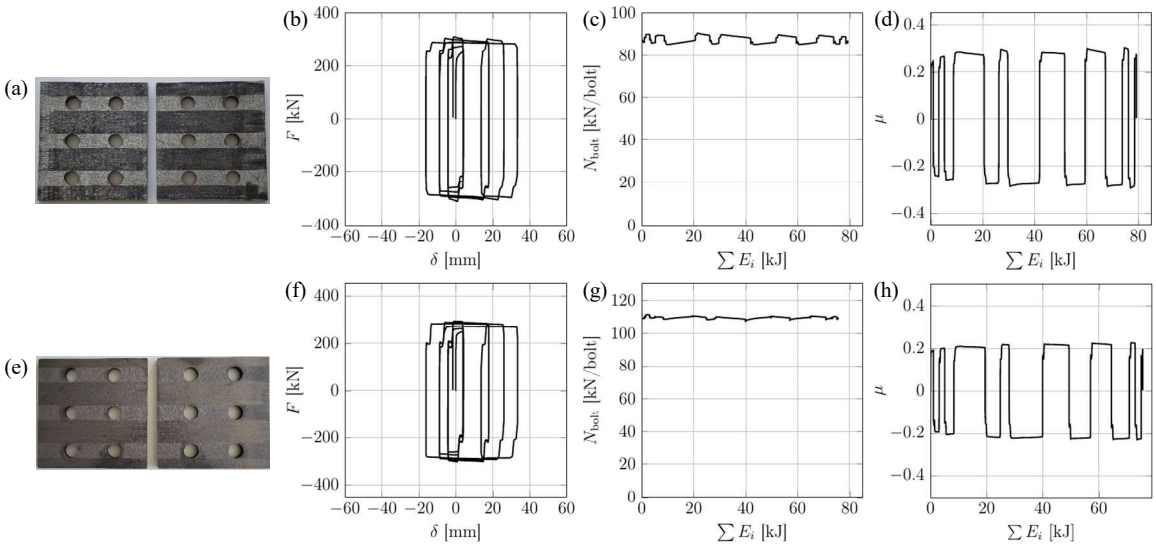

Fig. 10 – Results obtained for M1 (first row) and M2 (second row) under the pulse-like loading protocol and F_s = 300kN

4. Discussion

4.1 Pressure dependency

This section discusses the effect of the applied clamping force on the static friction coefficient of M1 and M2. Figures 11a and 11b illustrate the μ_s values obtained for different slip loads as a function of ΣE_i. The experimental results reveal that the static friction coefficient μ_s of M1 and M2 is somewhat pressure dependent. In order to evaluate the relevance of such a dependency, the mean, μ_μ, and standard deviation, σ_μ, of μ_s are computed. Figure 11c reveals that for both M1 and M2, μ_μ and σ_μ are smaller when the clamping force is doubled (i.e. for F_s = 300 kN). Notably, μ_μ shows a reduction of nearly 15% for both materials. While μ_s is somewhat pressure dependent, the corresponding percentage reductions of μ_μ are low. Consequently, we conclude that such a dependency is minor at pressures higher than 7-8 MPa. Furthermore, σ_μ assumes values smaller than 0.05 for both materials, i.e. μ_s is relatively stable under cyclic loading.

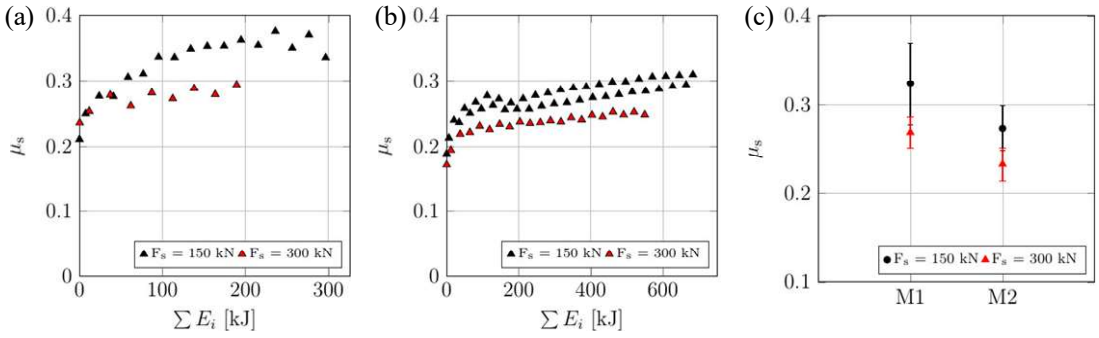

Fig. 11 – Static friction coefficient obtained under the cyclic loading protocol with constant amplitude: (a) μ_s obtained for M1, (b) μ_s obtained for M2, (c) mean and standard deviation of μ_s

4.2 Effect of loading rate

This section investigates the effect of the loading rate on the static friction coefficient of M1 and M2. Figure 12 illustrates the μ_s values obtained for F_s = 300 kN under different loading protocols and sliding velocities

v_s. The static friction coefficients considered hereafter correspond to the μ_d values obtained at the first sliding instant.

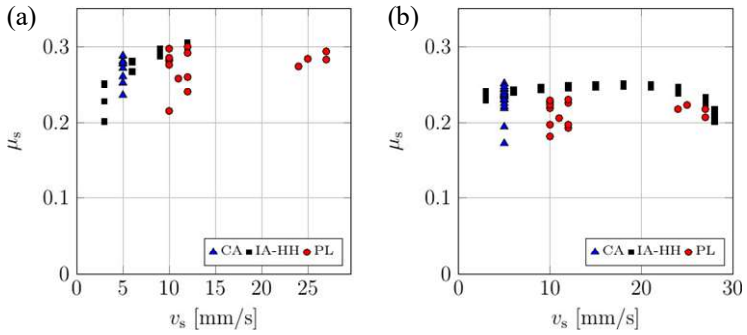

Fig. 12 – Static friction coefficient as a function of the sliding velocity obtained for the pulse-like loading protocol (PL), the cyclic loading protocol with constant (CA) and increasing amplitude (IA-HH): (a) friction pad M1, (b) friction pad M2

For M1, it is apparent that velocity-dependency is merely high at relatively low sliding velocities. Indeed, for v_s < 10 mm/s, μ_s increases with the sliding velocity, whereas it remains relatively constant at higher v_s values. As discussed in [17], μ is influenced by the strength properties of the respective materials in contact within the sliding interface. This suggests that the velocity-dependency identified in Fig. 12a is strongly related to them. Notably, it is reasonable to assume that M1 is characterized by a visco-plastic shear strength, i.e. its stress-strain response varies according to the imposed deformation rate [18]. Therefore, μ_s is loading-rate dependent [16]. However, this dependency vanishes at high sliding velocities (i.e. v_s > 10 mm/s), i.e. under conditions similar to those occurring during a seismic event, M1 can provide a relatively stable μ_s value.

With regard to M2, Fig. 12b reveals that μ_s starts decreasing progressively merely under the cyclic loading protocol with increasing amplitude (IA-HH) and for v_s > 25 mm/s. Indeed, under the pulse-like (PL) loading protocol, M2 provides relatively constant μ_s values regardless of the corresponding sliding velocity. This suggests that the decrease of μ_s observed in Fig. 12b is mainly attributed to the wearing process. The latter is more pronounced under the cyclic loading protocol with increasing amplitude (IA-HH) than under the pulse-like loading protocol because in the first case the cumulative displacement experienced by M2 is larger. Consequently, the static friction coefficient of M2 is velocity independent.

5. Summary and observations

The present paper discusses the results of an experimental campaign conducted on a sliding friction damper prototype. Two types of non-metallic friction pads have been tested at two different pressure levels and under three loading protocols. Their static and dynamic friction coefficients have been investigated in order to evaluate their applicability in the context of earthquake engineering. While the authors are still evaluating several aspects of the experimental program, the preliminary results, which are presented herein, suggest that:

- Both examined materials are characterized by similar static and dynamic friction coefficients, i.e. once the slip load is exceeded, the friction device slides under a relatively constant axial force.
- The friction coefficient of both friction pads is somewhat pressure dependent. However, such a dependency turns out to be minor at pressures higher than 7 to 8 MPa, which are typical for the range of anticipated sliding loads to be achieved with the damper prototype.
- Both materials provide stable μ values when they operate at sliding velocities larger than 10 mm/s, i.e. in this case the axial force - axial displacement hysteretic response of the sliding friction damper is stable and repeatable.

- At the end of each loading protocol, the surfaces of the pads appear strongly damaged due to surface wear compared to the inner steel plate surfaces. The observed damage pattern is insensitive to the imposed loading history.
- During a number of tests, some of the friction pads experienced net section fracture due to the associated reduction of the friction pad area because of surface wear. In the worst case, fracture occurs at ΣE_i = 120 kJ for M1, whereas this does not happen prior to ΣE_i = 500 kJ for M2. However, if this is a concern, fracture may be prevented by using a thicker friction pad.
- Under conditions potentially similar to those occurring during a seismic event (i.e. sliding velocity of 27 mm/s), M1 and M2 provide a static friction coefficient of about 0.28 and 0.22, respectively. These values are slightly lower compared to the target value of 0.30 established in Section 2.1.2. Nevertheless, the hysteretic response of the sliding friction damper is not compromised.

All-in-all, the authors think that the tested friction pads are promising for earthquake engineering applications with emphasis on the mitigation of seismic demands on structures. Therefore, their further investigation is recommended.

6. Acknowledgements

This study is based on work supported by the Swiss National Science Foundation (Project No. 200021_188476). The financial support is gratefully acknowledged. Any opinions, findings and conclusions expressed in the paper are those of the authors and do not necessarily reflect the views of sponsors. The authors would like to sincerely thank the technical staff at the EPFL Structures Laboratory: Léa Frédérique Dubugnon, Gilles Guignet and Serge Despont, as well as the undergraduate students: Cesar Daniel Ramirez Mendoza (summer intern from University of Texas at El Paso, USA), Nitesh Karmacharya (intern from University of Katmandu, Nepal) and graduate student Elias Merhi (EPFL, Switzerland) for their invaluable assistance during the testing program.

7. References

[1] Aiken, I. D., Nims, D. K., Whittaker, A. S. & Kelly, J. M. (1993), Testing of passive energy dissipation systems, *Earthquake Spectra* **9**(3), 335–370.

[2] Tirca, L. (2015), Friction Dampers for Seismic Protections of Steel Buildings Subjected to Earthquakes: Emphasis on Structural Design, *Springer Berlin Heidelberg*, Berlin, Heidelberg, pp. 1058–1070.

[3] Pall, A. S. (1979), Limited slip bolted joints: a device to control the seismic response of large panel structures, PhD thesis, Concordia University.

[4] Grigorian, C. E., Yang, T.-S. & Popov, E. P. (1993), Slotted bolted connection energy dissipators, *Earthquake Spectra* **9**(3), 491–504.

[5] Golondrino, J. C., MacRae, G. & Clifton, C. (2012), Behaviour of asymmetrical friction connections using different shim materials, *in* 'Proceedings of the New Zealand Society for Earthquake Engineering Conference'.

[6] Khoo, H.-H., Clifton, C., Butterworth, J., MacRae, G. & Ferguson, G. (2012), Influence of steel shim hardness on the sliding hinge joint performance, *Journal of Constructional Steel Research* **72**, 119–129.

[7] Latour, M., Piluso, V. & Rizzano, G. (2014), Experimental analysis on friction materials for supplemental damping devices, *Construction and Building Materials* **65**, 159–176.

[8] MacRae, G. A., Clifton, G. C., Mackinven, H., Mago, N., Butterworth, J. & Pampanin, S. (2010), The sliding hinge joint moment connection, *Bulletin of the New Zealand Society for Earthquake Engineering* **43**(3), 202–212.

[9] Ono, S., Nakahira, K., Tsujioka, S. & Uno, N. (1996), Energy absorption capacity of thermally sprayed aluminum friction dampers, *Journal of Thermal Spray Technology* **5**(3), 303–309.

[10] Latour, M., Piluso, V. & Rizzano, G. (2016), Experimental analysis and design of friction joints equipped with sprayed aluminum dampers, *in* 'Proceedings of the 8th International Workshop on Connections in Steel Structures, Boston, USA, May', pp. 619–630.

[11] Golondrino, J. C., MacRae, G., Chase, J., Rodgers, G. & Clifton, C. (2012), Clamping force effects on the behaviour of asymmetrical friction connections (afc), *in* 'Proceedings of the 15th World Conference on Earthquake Engineering (15WCEE), Lisbon, Portugal, September', pp. 24–28.

[12] Tsampras, G. & Sause, R. (2015), Development and experimental validation of deformable connection for earthquake-resistant building systems with reduced floor accelerations, *Network of Earthquake Engineering Simulation (NEES) Technical Report, https://nees. org/resources/13612*.

[13] SIA 263 (2013), *Steel structures*, Swiss Society of Engineers and Architects (SIA), Zurich.

[14] Persson, B. N. (2013), *Sliding friction: physical principles and applications*, Springer Science & Business Media.

[15] Rabinowicz, E. (1995), *Friction and wear of materials*, 2nd edition, Wiley & Sons, New York.

[16] Lemaitre, J. (2001), *Handbook of Materials Behavior Models, Three-Volume Set: Nonlinear Models and Properties*, Elsevier.

[17] Bowden, F. P. & Tabor, D. (1973), *Friction: an introduction to tribology*, RE Krieger Publishing Company.

[18] François, D., Pineau, A. & Zaoui, A. (1998), *Mechanical behaviour of materials: Volume II: Viscoplasticity, Damage, Fracture and Contact Mechanics*, Springer Science & Business Media.

